Article:
Wang, Q, Polansky, J, Wang, M et al. (4 more authors) (2018) Capability of dual-modality electrical tomography for gas-oil-water three-phase pipeline flow visualisation. Flow Measurement and Instrumentation, 62. pp. 152-166. ISSN 0955-5986

https://doi.org/10.1016/j.flowmeasinst.2018.02.007

Capability of Dual-Modality Electrical Tomography for Gas-oil-water Three-phase Pipeline Flow Visualisation

Qiang Wang[a], Jiri Polansky[a], Mi Wang[a,*], Kent Wei[b], Changhua Qiu[b], Asaad Kenbar[c], David Millington[c]

[a] *School of Chemical and Process Engineering, University of Leeds, Leeds LS2 9JT, UK*
[b] *Industrial Tomography System plc, Manchester M3 3JZ, UK*
[c] *TUV NEL, Glasgow, G75 0QF, UK*

Abstract

Numerous dual-modality tomography systems have previously been studied for the application of multiphase flow characterisation, however, the capability of the majority of these systems was only demonstrated under limited flow regime conditions, such as stratified flow and slug flow. This paper reports a dual-modality electrical tomography for visualisation of industrial-scale, horizontal gas-oil-water three-phase flows. Experimental conditions include water-to-liquid ratio (WLR) from 0% to 100% in parallel with gas volume fractions (GVF) from 0% to 100%, which produced a variety of flow patterns, typically stratified flow, slug flow, plug flow, bubbly flow, and annular flow. A commercial dual-modality electrical tomographic system was utilised to carry out the flow structure measurement. A threshold-based data fusion method was also deployed for the fusion of oil-continuous and water-continuous data to provide full three phase images. The tomography visualisation is validated against optical photographs derived from a high-speed video logger located shortly upstream of the device. The results demonstrate that a subcomponent of the dual modality sensor, an electrical resistance tomography (ERT) system, is able to visualise water continuous flow with WLR higher than 40%, providing good agreement with previous reports. The remaining subcomponent, the electrical capacitance

*Corresponding author
Email address: m.wang@leeds.ac.uk (Mi Wang)

tomography (ECT) system, is able to provide stable measurement during WLR from 0% to 90%, which is far beyond initial expectations and previous findings. Mean concentrations measured with the dual-modality system reveal the potential capability of the tomography system for phase fraction measurement. The visualisation results with the advanced data fusion method and mean concentration measurement verify the capability of the system in the application of gas-oil-water flow characterisation.

Keywords: electrical resistance tomography (ERT), electrical capacitance tomography (ECT), dual-modality ERT-ECT systems, gas-oil-water horizontal flow, three-phase flow visualisation, multi-dimensional data fusion

---

As a common phenomenon in many industries, three-phase flow has attracted much attention from researchers and engineers. It is however extremely challenging to measure and visualise such phenomenon, due to the complex interactions between each phase, with over 20 different flow regimes having been observed [1, 2]. In order to provide insights into gas-oil-water flow, many techniques have been commercially applied and scientifically proposed in the past few decades [3], among which multi-modality tomographic systems have been suggested to be effective in several multiphase flow applications, with the advantages of being low cost, non-intrusive/invasive, and robust. [4, 5].

Multi-modality tomographic systems, as the name indicates, integrate different modalities of tomography to overcome the incapability of single-modality tomographic systems when more than two components are engaged in the investigated flow. They usually distinguish different phases or phase combinations by each modality by applying specific data fusion based on the results from both modalities. Taking an ERT-ECT systems as an example, ERT is able to identify conductive phase, i.e. water in gas-oil-water flow, and non-conductive phase, i.e. gas and oil in gas-oil-water flow, whereas ECT is able to distinguish gas from liquid, i.e. water and oil, in the gas-oil-water flow [6].

So far, varieties of multi-modality tomographic systems have been proposed for the purpose of three-phase flow measurement and visualisation. A particu-

lar instance of dual-modality tomography is dual-modality electrical tomography that integrates electrical resistance and capacitance tomography together for the quantification and qualification of multiphase flow regimes. Several reports are dedicated to the design and prototyping of such systems. Although there are differences with some aspects, e.g. using two standalone modalities to obtain the conductivity and permittivity distributions separately ([6, 11]), or using integrated sensing electrodes to measure once and derive both distributions ([12, 13, 14]). Conventional ERT-ECT systems offer cross-sectional images of high temporal resolution but relatively low spatial resolution. A major barrier for the systems is that they are unable to identify small bubbles, as well as produce sharp interfaces between large bubbles and liquid phase within multiphase flow, due to the non-linear distribution of the induced electrical field for sensing and associated ill-conditioned inverse problems in image reconstruction. In addition, multiphase flow imaging is not only for human/machine perception, but also requires quantitative results, e.g. concentration distribution, to convey sufficient information in regard to flow dynamics, and to obtain comparative analysis of the performance of such systems. Unfortunately, nonlinearity of electrical tomography imaging exists, particularly for a large change in electric or dielectric property. All these limitations and unique characteristics introduce some technical challenges into the application of the systems for multiphase flow visualisation. For example, contemporary data fusion algorithms in medical imaging [15] may not be applicable to the fusion process in ERT-ECT systems.

Although multi-modality tomographic systems have attracted much attention, the data fusion methods are still at an early stage of research and development. Reported evaluations have been conducted using either simulation techniques or simple flow structures, e.g. stratified flow [6, 8, 13]. Although Yue *et al.* have assessed their ERT-ECT systems for several flow regimes in laboratory-scale gas-water two-phase flow facilities, for a variety of stratified flow, slug flow, and plug flow, the capability of systems for extensive flow regimes of gas-oil-water flow is still unknown. Despite the success of the proposal by

Wang *et al.* in [10] for water-continuous three-phase flow, their system is unable to distinguish gas and oil phase, and hence only able to distinguish conductive phase (water) and non-conductive phase (gas and oil).

This paper reports the experimental evaluation of dual-modality ERT-ECT systems on the basis of the experiments conducted at the industrial-scale multiphase flow facility at TUV NEL[1]. The flow conditions tested included WLR from 0% to 100% associated with GVF from 0% to 100%, which produces common horizontal flow regimes [16], including stratified flow, slug flow, plug flow, bubbly flow, and annular flow. The evaluation aims to investigate capability of the ERT-ECT dual-modality systems on both qualitative and quantitative bases, by means of images and mean concentrations, respectively. The outcome investigation and capability of the ERT-ECT systems as single- and dual-modality tomographic systems iare discussed in correspondence with the evaluation results in below sections.

The paper is organised as follows. The principle of electrical tomography is briefed in Section 1. Section 2 introduces the details of the experimental setup. The evaluation results are presented in Section 3, and discussed in Section 4. Final conclusion is made in Section 5.

1. Electrical tomography

Electrical tomography is a technique that is based on electromagnetic principles to sense electrical property distribution within an interested domain. Depending on its operational principles, the different approach concerns different sensitive interests. For example, ERT measures the conductivity changes over a sensing domain, whereas ECT gauges permittivity differences within a sensing field. In principle, since there is no current sources within the pipeline, the electrical field distribution of ERT and ECT is governed by the same equation

[1] http://www.tuvnel.com

form:

$$\nabla \cdot (x \nabla \phi) = 0 \tag{1}$$

where x denotes either the permittivity of dielectric property ε in ECT or the conductivity of electrical property σ in ERT. Because of the similarity in governing equation, the solutions for both modalities also share some common features. A simple inverse solution is the single-step linear back-projection [17] in both ERT and ECT, which is widely applied to online monitoring owing to its computational simplicity. There are also advanced algorithms to solve inverse problems, such as iterative methods [18, 19], which yield more precise outcome but usually require more time and computational resources. Detailed discussion in regard to hardware and image reconstruction can be found from other sources [5, 19, 20].

After the reconstruction, interested materials may be revealed by means of electrical property distribution, such as conductivity for ERT and permittivity for ECT. Conductivity distribution can be further converted to concentration distribution using Maxwell equation [21]:

$$\alpha = \frac{2\sigma_1 + \sigma_2 - 2\sigma_{mc} - \frac{\sigma_{mc}\sigma_2}{\sigma_1}}{\sigma_{mc} - \frac{\sigma_2}{\sigma_1}\sigma_{mc} + 2(\sigma_1 - \sigma_2)} \tag{2}$$

Where α is the void fraction of non-conductive component, σ_1 is the conductivity of conductive component, σ_2 is the conductivity of non-conductive component, and σ_{mc} is the reconstructed conductivity. Similarly, permittivity distribution can be also mapped to concentration distribution.

Due to their distinct sensing properties, ERT and ECT are employed simultaneously to differentiate multiple components. Under the condition of gas-oil-water multiphase flow, it is expected ERT to be able to extract gas and oil (non-conductive phase) information from water (conductive phase), whereas ECT is able to separate gas void fractin information from oil and water due to permittivity difference. Using proper decomposition approaches, individual phase distributions might be derived, and therefore insightful flow information can be provided.

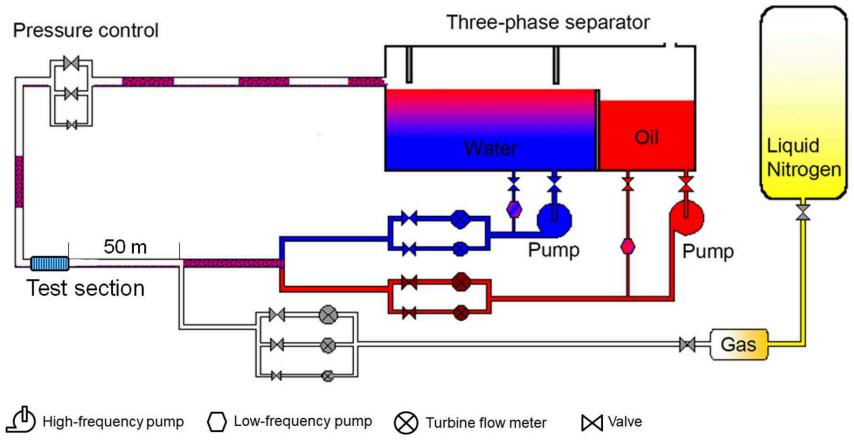

Figure 1: Schematic of NEL Multiphase Flow Facility [22].

Table 1: Physical properties of each phase.

	Gas	Oil	Water
Fluid	Nitrogen	Paraflex	Salty water
Conductivity (mS/cm)	0	0	33.5
Dielectric constant (ε)	1	2.2	80
Dynamic viscosity (cP)	0.0174	16.18	1.35
Density (kg/m^3)	12	830	1049.1

2. Experimental setup

The NEL multiphase flow loop is a three component flow facility featuring oil, water and gas. For measurement purposes, Paraflex (HT9) oil is used alongside substitute salt water (Magnesium Sulphate MgSO4) and a dry gas (Nitrogen) is injected externally via a pressurised storage tank. The physical properties of each phase are listed in Table 1. Each component is measured individually using reference turbine flow meters prior to being combined into a multiphase mixture. A 4-inch pipe was deployed for the experiments. On the test section, the dual-modality electrical tomography was mounted, after an inspection chamber for a high-speed camera to log flow structures as reference. The test section was

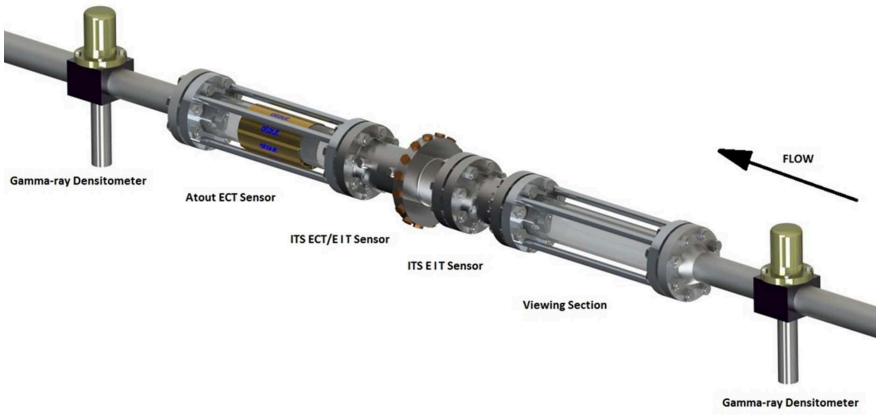

Figure 2: Test Section Line Build Schematic [22].

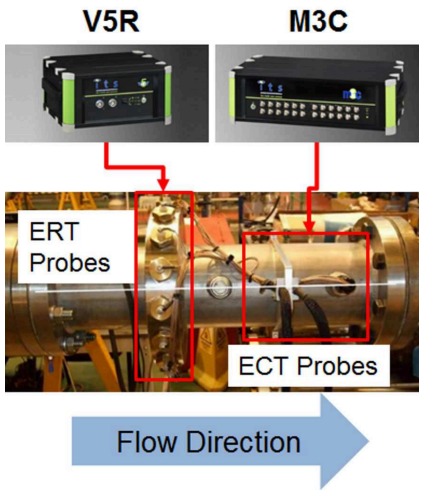

Figure 3: Dual-modality ERT-ECT systems employed in the research [22].

positioned approximately 50 meters away from component injection points, in order to let flow fully develop in the test section. After passing through the test section, the multiphase flow is then separated via a gravity separation vessel whereby the oil and water is re-circulated and nitrogen is expelled to atmosphere. A graphical representation of the flow facility is shown in Figure 1.

The testing objective was to evaluate the functional performance of the dual-

Table 2: Operation specification of the ERT-ECT system [22].

	V5R	M3C
Sensor configuration	2 planes of 16 electrodes	1 plane of 12 electrodes
Sensing strategy	Voltage-driven adjacent	Voltage-driven sequential
Injection frequency	10 KHz	1000 KHz
Reconstruction	Linear back projection (LBP)	Linear back projection (LBP)
Property of interest	Electrical conductivity	Electrical permittivity
Max acquisition speed	0.0016 s/Frame	0.08 s/Frame
Image grid	20×20	32×32
Image spatial resolution	5%	5%

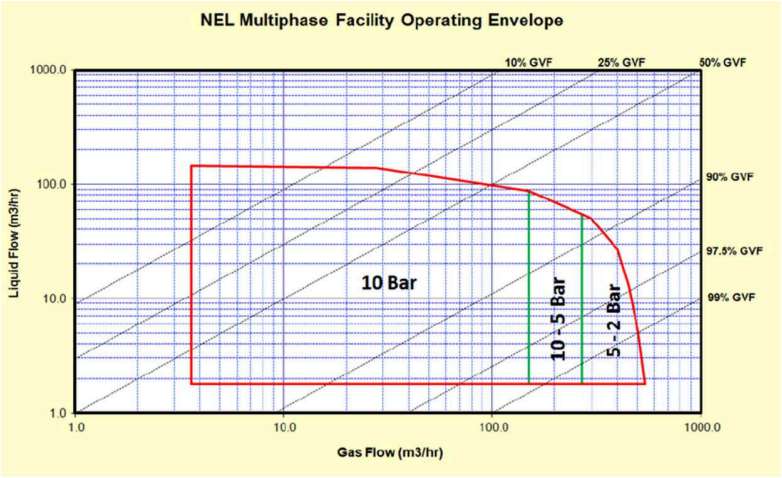

Figure 4: NEL flow facility operational envelope [22].

modality ERT-ECT systems in terms of multiphase flow visualisation. Several reference devices were installed in the test section, and the arrangement of the reference equipment is illustrated in Figure 2. In this experiment, ITS dual-modality systems were employed (Figure 3), including V5R ERT [23] system and M3C ECT system [6]. The detailed operational information of the dual-modality system is listed in Table 2.

Liquid flow rates of the NEL multiphase flow loop can reach 145 m^3/h while

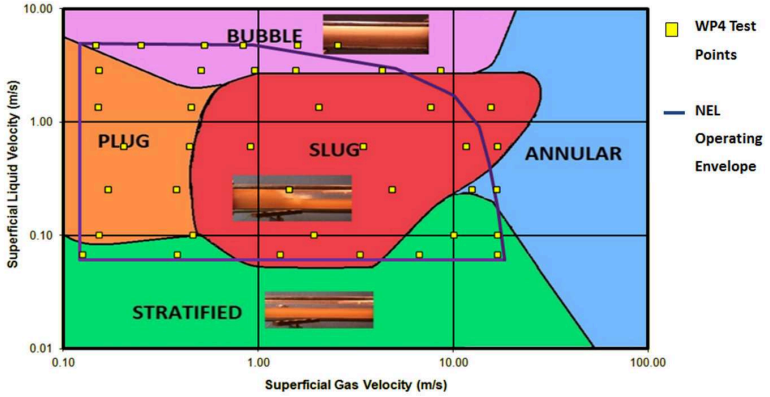

Figure 5: Targeting flow patterns [22].

gas can achieve 1500 m^3/h. Maximum gas flow rate is subject to operating pressure as the flow is a function of differential between gas injection pressure and line pressure. The flow loop is rated to 18.2 bar(g) with a maximum line pressure of 15 bar(g). The operating envelope is displayed in Figure 4. The facility can achieve GVF's and WLR's from 0% to 100%. The target flow patterns are shown in Figure 5, and flow conditions in terms of GVF and liquid flowrate are listed in Table 3. Hereafter, GVF, liquid flowrate, WLR, and phase flowrates are referring to measurement obtained or calculated from the reference facility except those specified as ERT, ECT, or Gamma-ray densitometer.

3. Experimental results

The results, grouped by WLR, are in two formats: one is qualitative, i.e. visualisation using axially-stacked images, and the other is quantitative, i.e. mean concentration.

As far as the visualisation is concerned, the images are produced from the ECT, the ERT and the data fusion, along with the images from a high-speed video logger as a visual reference. For the axially-stacked images, the X-axis represents the temporal information of the tomograms, i.e. a sequence of the tomograms at a specific data collection rate as given in Table 2, while Y axis

Table 3: Selected test conditions of liquid flowrate and GVF [22].

	Liquid flowrate (m3/h)						
GVF (%)	2	3	7.5	18	40	85	140
3							x
5						x	x
10							x
15						x	x
25				x	x	x	x
35						x	x
40			x				
42			x				
60							
75						x	
82		x				x	
85	x		x	x	x		
92					x		
95	x	x	x	x			
96.5				x			
98	x		x				
99	x	x	x				

represents the spatial information of the tomograms, i.e. the concentration distribution of a tomogram along the vertical diameter of the pipe, where 0 is the top and 60 is the bottom of the pipe [24]. Due to the capability of the video logger and the limited length of the available inspection chamber, full features of some flow conditions, e.g. long slug bubbles, may not be captured fully. Therefore, some reference images by the logger are stacked with several consecutive images. Some axially-stacked tomograms are extracted from a certain number of the original electrical concentration tomograms so that the visual comparison is more meaningful, e.g. slug flow and plug flow, whereas the others are pre-

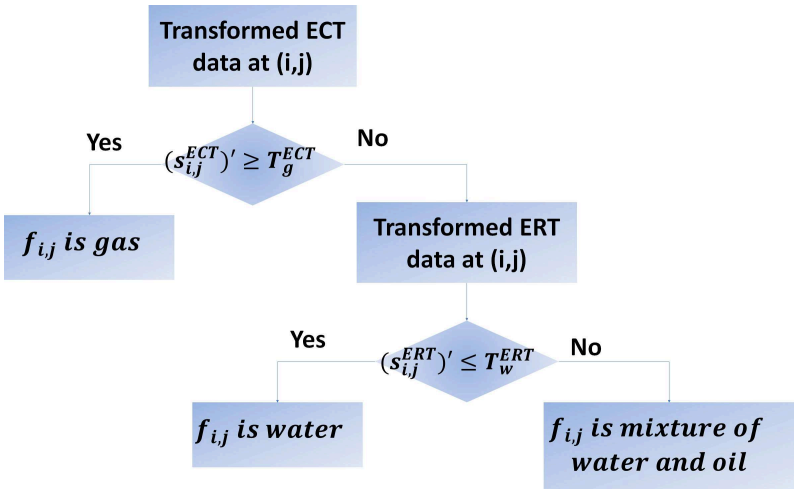

Figure 6: Data flow of the threshold-based fusion method [24].

sented using 1000 concentration tomograms by default. Due to the considerable amount of flow conditions, only five flow conditions are selected for demonstrating purpose, which represent five typical flow regimes, namely stratified flow, slug flow, plug flow, annular flow, and bubbly flow.

The threshold-based methodology for data fusion purpose of ERT-ECT systems were reported [6, 13], but only applied to simple stratified flow patterns. An advanced threshold-based data fusion method was developed, which can be applied to these five flow pattern [24]. Since concentration tomograms were obtained with ERT and ECT at different sampling speeds and different grid definitions in the research, they needed to be transformed so that they were space- and time- aligned before a pixel-by-pixel fusion algorithm performed. Later, two threshold values derived from empirical and experimental knowledge were used to binarise the concentration tomograms of ERT and ECT. One threshold value of 0.5 differentiated gas from the liquid phase in ECT tomograms. When the liquid phase was distinguished, the other threshold value of 0.5 was applied to the ERT tomograms to separate oil and water. If the pixel value was greater than 0.5, the liquid is assumed to be oil, or otherwise water. Finally, pixel values were generated by integrating the threshold values along registered ERT and

ECT tomograms. The fusion process is depicted in Figure 6, and the technical detail is described in [24].

Quantitative results are compared in terms of water and gas mean concentrations. However, the primary objective of the project is visualisation. Volumetric fraction values, i.e. WLR and GVF, are utilised directly as one of correlations for evaluating the mean concentrations of water and gas obtained with the ERT-ECT under a condition of lacking effective method to evaluate these local concentrations obtained from the ERT-ECT. For water concentration, three values are presented, including the reference value by Equation 3, mean concentration from the ERT using Equation 4, and the one from data fusion results.

$$\overline{\alpha}_w^{ref} = \frac{(100 - GVF) * WLR}{100} \tag{3}$$

$$\overline{\alpha}_w^{ERT} = 100 - \overline{\alpha}^{ERT} \tag{4}$$

where $\overline{\alpha}^{ERT}$ is the mean concentration of disperse phase by ERT.

For gas concentration, four results are compared, i.e. the GVF, mean concentration derived from Equation 5,Equation 6, and Equation 7 gamma-ray densitometer, mean concentration from the ECT, and the one using the data fusion. Since gas concentration by the data fusion is determined solely by the ECT, the ECT results and corresponding data fusion approach are identical, and hence reflected as one value. The mixture density by gamma-ray is as below:

$$\rho_m = \rho_g * \alpha_g + \rho_w * \alpha_w + \rho_o * \alpha_o \tag{5}$$

Where ρ_x is the density for each phase or the mixture, and α_x is the volume fraction of each phase. Compared to ρ_w and ρ_o, the ρ_g is so small that it can be ignored. In addition, ρ_w and ρ_o are approximated using density of liquid ρ_l, of which the value is replaced by water density ρ_w. Consequently, Equation 5 is changed to

$$\rho_m \approx \alpha_l * \rho_w \Rightarrow \alpha_l \approx \frac{\rho_m}{\rho_w} \tag{6}$$

Table 4: Selected flow conditions for visualisation at WLR 0%.

	GVF (%)	Q_{oil} (m^3/h)	Q_{gas} (m^3/h)
Stratified flow	97	2.948	94.640
Slug flow	42	17.890	13.009
Plug flow	25	39.334	13.298
Annular flow	95	18.023	340.655
Bubbly flow	25	139.360	47.466

Further, gas volume fraction can be calculated by Equation 7:

$$\alpha_g \approx 1 - \alpha_l \approx 1 - \frac{\rho_m}{\rho_w} \tag{7}$$

On the other hand, new references were taken for the ERT and the ECT at each WLR, in order to improve the accuracy of the measurements. For ERT, the salty water was used for the reference, whereas for the ECT, fully dispersed oil-water flow at given WLR and 0% GVF was used as the reference.

The reference GVF and WLR are calculated from the phase flowrates at the feed-in point of the flow test rig. The concentrations obtained from Gamma-ray densitometer, ERT and ECT are measured at the their sensors locations at the test section as shown in Figure 1 and Figure 2. In principle, the local phase concentrations may not be the same as the references unless phase slip velocities ignorable. However, at the absence of relevant local references, we summarise the flow feed-in references and local measurements together in below results to reflect their correlations.

3.1. WLR 0%

At WLR 0%, in total 42 different flow conditions were examined, covering all common flow regimes in a horizontal pipeline [16]. Since WLR is 0%, i.e.

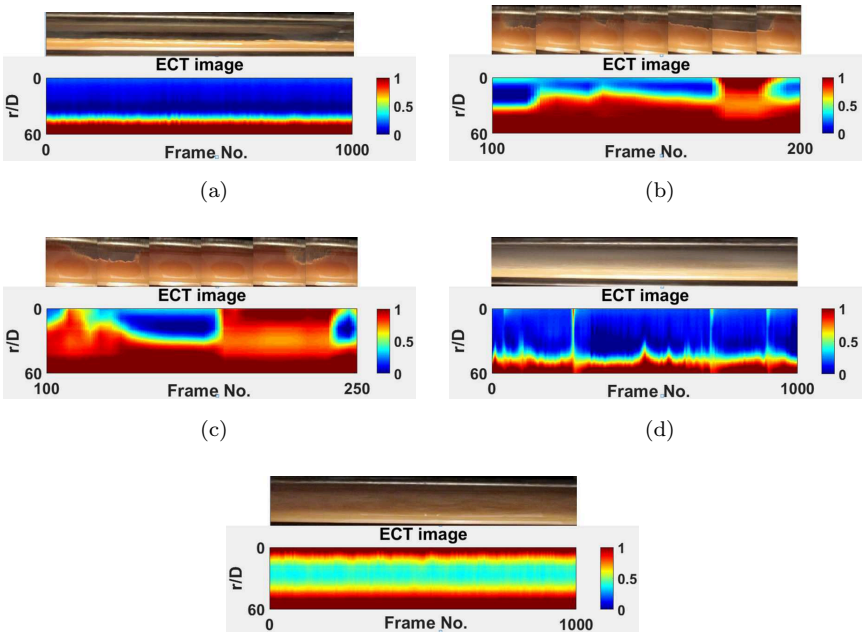

Figure 7: Visualisation results of WLR 0% for (a) stratified flow; (b) slug flow; (c) plug flow; (d) annular flow; and (e) bubbly flow.

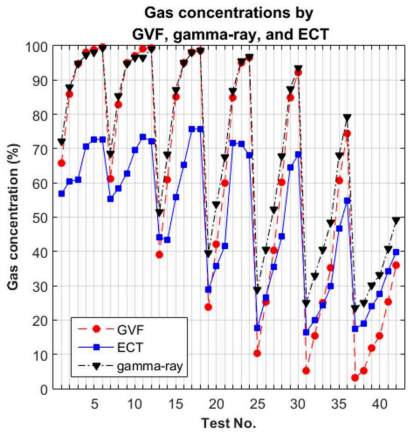

Figure 8: Gas concentrations from different approaches at WLR 0%.

gas-oil two-phase flow, which is beyond the ERT's measurable range, only the stacked ECT tomograms are presented, along with the images taken using high-

Table 5: All examined flow conditions at WLR 0%.

Test No.	GVF %	ERT %	ECT %	Data fusion (%) gas	oil	water	Gammy %	Flow Regimes
1	65	x	56.78	x	x	x	72.11	stratified
2	85	x	60.51	x	x	x	87.89	stratified
3	95	x	60.82	x	x	x	94.75	stratified
4	98	x	70.69	x	x	x	97.24	stratified
5	99	x	72.74	x	x	x	98.10	stratified
6	99.6	x	72.69	x	x	x	99.37	transition
7	60	x	55.44	x	x	x	68.65	stratified
8	82	x	58.38	x	x	x	85.45	stratified
9	95	x	62.76	x	x	x	94.89	stratified
10	97	x	69.50	x	x	x	96.44	stratified
11	99	x	73.46	x	x	x	96.44	stratified
12	99.4	x	72.07	x	x	x	99.21	transition
13	40	x	44.03	x	x	x	51.50	stratified
14	60	x	43.46	x	x	x	68.39	transition
15	85	x	55.73	x	x	x	87.27	slug
16	95	x	65.32	x	x	x	94.97	transition
17	98	x	75.72	x	x	x	98.00	annular
18	98.5	x	75.72	x	x	x	98.50	annular
19	25	x	28.87	x	x	x	39.55	slug
20	42	x	35.78	x	x	x	53.73	slug
21	60	x	41.57	x	x	x	67.54	slug
22	85	x	71.61	x	x	x	86.98	annular
23	95	x	71.35	x	x	x	95.55	annular
24	96.5	x	68.10	x	x	x	96.87	annular
25	10	x	17.68	x	x	x	28.93	plug
26	25	x	26.50	x	x	x	40.62	plug
27	40	x	35.49	x	x	x	52.40	transition
28	60	x	44.38	x	x	x	67.91	slug
29	85	x	64.38	x	x	x	87.46	slug
30	92	x	68.19	x	x	x	93.57	transition
31	5	x	16.53	x	x	x	25.16	bubbly
32	15	x	19.91	x	x	x	33.06	slug
33	25	x	24.28	x	x	x	40.51	slug
34	35	x	29.79	x	x	x	48.40	slug
35	60	x	46.57	x	x	x	68.19	transition
36	75	x	54.95	x	x	x	79.26	annular
37	3	x	17.52	x	x	x	23.57	bubbly
38	5	x	18.93	x	x	x	25.05	bubbly
39	10	x	24.02	x	x	x	30.16	bubbly
40	15	x	27.63	x	x	x	33.13	bubbly
41	25	x	34.31	x	x	x	40.81	bubbly
42	35	x	39.90	x	x	x	49.13	bubbly

speed video, as depicted in Figure 7, and all flow conditions selected are listed in Table 5. The Flow conditions for demonstrating the capability of the ECT are

Table 6: Selected flow conditions for visualisation at WLR 10%.

	GVF (%)	Q_{water} (m^3/h)	Q_{oil} (m^3/h)	Q_{gas} (m^3/h)
Slug flow	85	2.178	18.451	103.398
Plug flow	15	8.877	76.756	14.759
Annular flow	75	2.211	18.214	495.811
Bubbly flow	5	14.544	124.980	7.161

listed in Table 4. From a visualisation point of view, the ECT tomograms agree well with the videos, except the ones for bubbly flow as shown in Figure 7e. This is because the ECT utilised is unable to identify small bubbles of a size very much smaller than pipe diameter. On the other hand, Figure 8 presents the quantitative comparison of the ECT results with the results by GVF and gamma-ray. Since the ERT part in the dual-modality system is not functional, the quantitative result only compares gas concentrations by GVF, gamma-ray, and the ECT.

3.2. WLR 10%

With WLR at 10%, 16 different flow conditions were tested, as listed in Table 7. Due to the limited number of flow conditions, the facility did not manage to produce all common flow regimes. The visualisation results illustrated in Figure 9 involve only four flow regimes, i.e. slug, plug, annular, and bubbly flow, of which the flow conditions are itemised in Table 6. Similar to the situation at WLR 0%, the ERT is still incapable of generating acceptable images. As far as imaging is concerned, the ECT is generally able to provide reasonable results, as presented in Figure 9. It is, however, also noticed that in 9c, the ECT struggles to identify the liquid film at the top of the pipe wall. This is primarily because the film is too thin to be identifiable, which suggests the thinness is

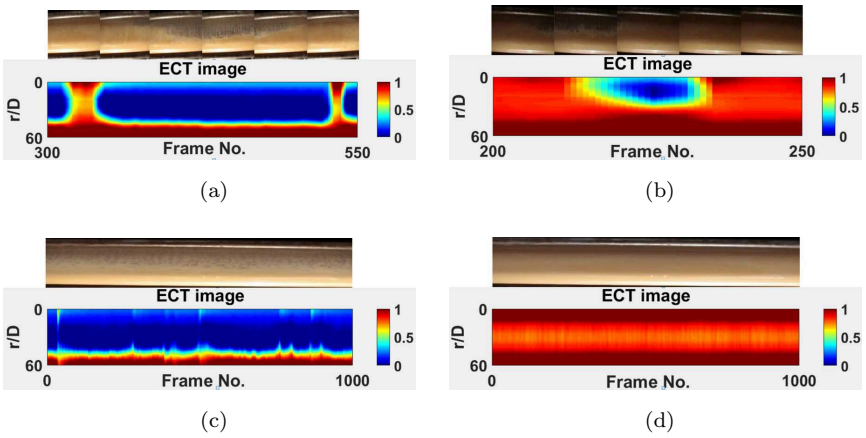

Figure 9: Visualisation results of WLR 10% for (a) slug flow; (b) plug flow; (c) annular flow; and (d) bubbly flow.

Table 7: All examined flow conditions at WLR 10%.

Test No.	GVF %	ERT %	ECT %	Data fusion (%) gas	oil	water	Gammy %	Flow Regimes
1	60	x	47.13	x	x	x	63.71	slug
2	85	x	63.07	x	x	x	85.52	slug
3	95	x	71.06	x	x	x	94.33	transition
4	96.5	x	74.16	x	x	x	96.46	annular
5	5	x	11.01	x	x	x	23.31	bubbly
6	15	x	18.21	x	x	x	30.62	plug
7	25	x	25.26	x	x	x	39.21	transition
8	35	x	32.22	x	x	x	46.64	transition
9	60	x	50.71	x	x	x	66.46	slug
10	75	x	59.49	x	x	x	77.52	transition
11	3	x	9.29	x	x	x	21.00	bubbly
12	5	x	12.92	x	x	x	22.79	bubbly
13	10	x	17.43	x	x	x	27.25	bubbly
14	15	x	21.33	x	x	x	30.40	bubbly
15	25	x	31.18	x	x	x	38.68	bubbly
16	35	x	38.31	x	x	x	45.53	bubbly

below the resolution of the ECT [6]. Figure 10 presents the comparison of gas concentrations by GVF, gamma-ray, and the ECT.

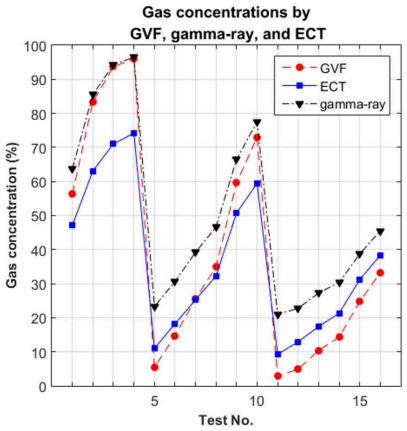

Figure 10: Gas concentrations from different approaches at WLR 10%.

Table 8: Selected flow conditions for visualisation at WLR 25%.

	GVF (%)	Q_{water} (m^3/h)	Q_{oil} (m^3/h)	Q_{gas} (m^3/h)
Slug flow	40	10.635	31.481	26.505
Annular flow	92	10.213	28.840	458.146
Bubbly flow	10	35.406	105.336	16.833

3.3. WLR 25%

Given WLR at 25 %, 21 flow conditions were involved in the experiment, which however only reflect three flow regimes, including slug, annular, and bubbly flow. Figure 11 depicts the selected visualisation results in line with the conditions in Table 8. The whole set of the conditions examined at WLR 25 % is listed in Table 9. Similar to the results for WLR 0% and 10%, the ECT tomograms are generally consistent with video footage, except for bubbly flow. Figure 11b shows an interesting phenomenon, i.e. the thickness of the liquid film at the top of the pipe changes almost periodically, implying that the flow was fully developed, and hence at steady state. The gas concentrations calculated by GVF, gamma-ray, and the ECT, are demonstrated in Figure 12.

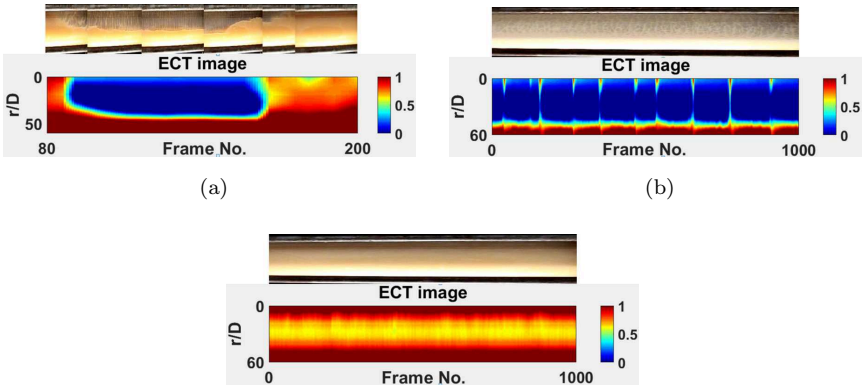

Figure 11: Visualisation results of WLR 25% for (a) slug flow; (b) annular flow; and (c) bubbly flow.

Table 9: All examined flow conditions at WLR 25%.

Test No.	GVF %	ERT %	ECT %	Data fusion (%) gas	oil	water	Gammy %	Flow Regimes
1	95	x	80.14	x	x	x	94.40	transition
2	98	x	79.31	x	x	x	97.31	transition
3	98.5	x	81.52	x	x	x	98.16	annular
4	85	x	69.38	x	x	x	85.43	slug
5	95	x	75.04	x	x	x	95.34	transition
6	96.5	x	75.04	x	x	x	96.73	annular
7	25	x	44.89	x	x	x	36.83	slug
8	40	x	37.93	x	x	x	47.83	slug
9	60	x	47.62	x	x	x	64.45	transition
10	85	x	67.72	x	x	x	85.71	annular
11	92	x	74.59	x	x	x	93.03	annular
12	5	x	10.03	x	x	x	20.09	bubbly
13	15	x	19.37	x	x	x	28.87	transition
14	25	x	31.47	x	x	x	37.36	transition
15	35	x	36.59	x	x	x	44.42	transition
16	60	x	54.53	x	x	x	65.45	transition
17	75	x	62.09	x	x	x	77.61	annular
18	3	x	15.08	x	x	x	18.39	bubbly
19	5	x	16.16	x	x	x	19.94	bubbly
20	10	x	21.34	x	x	x	24.70	bubbly
21	15	x	27.21	x	x	x	28.63	bubbly

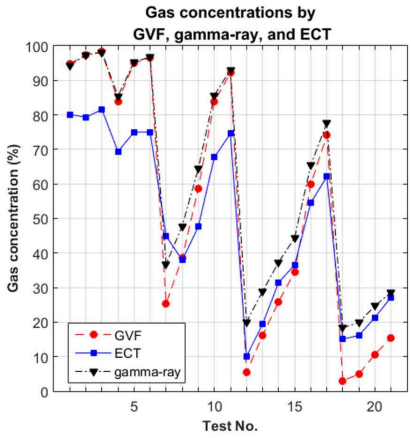

Figure 12: Gas concentrations from different approaches at WLR 25%.

Table 10: Selected flow conditions for visualisation at WLR 50%.

	GVF (%)	Q_{water} (m^3/h)	Q_{oil} (m^3/h)	Q_{gas} (m^3/h)
Stratified flow	60	3.790	3.860	10.978
Slug flow	60	9.031	9.030	27.896
Plug flow	25	42.520	40.626	27.841
Annular flow	75	42.451	40.974	254.034
Bubbly flow	5	70.327	69.061	7.606

3.4. WLR 50%

There were 29 flow conditions at 50% WLR. The selected flow conditions from the full set (Table 11) are listed in Table 10 and the associated images are presented in Figure 13. Since ERT is fully operational at 50% WLR, the visualisation results are presented using the tomograms by the ECT, the ERT, and the data fusion approach, in parallel with the images by high-speed video logger as a reference. Figure 13 illustrates the results. From the visualisation perspective, the figures demonstrate a promising capability of the systems for

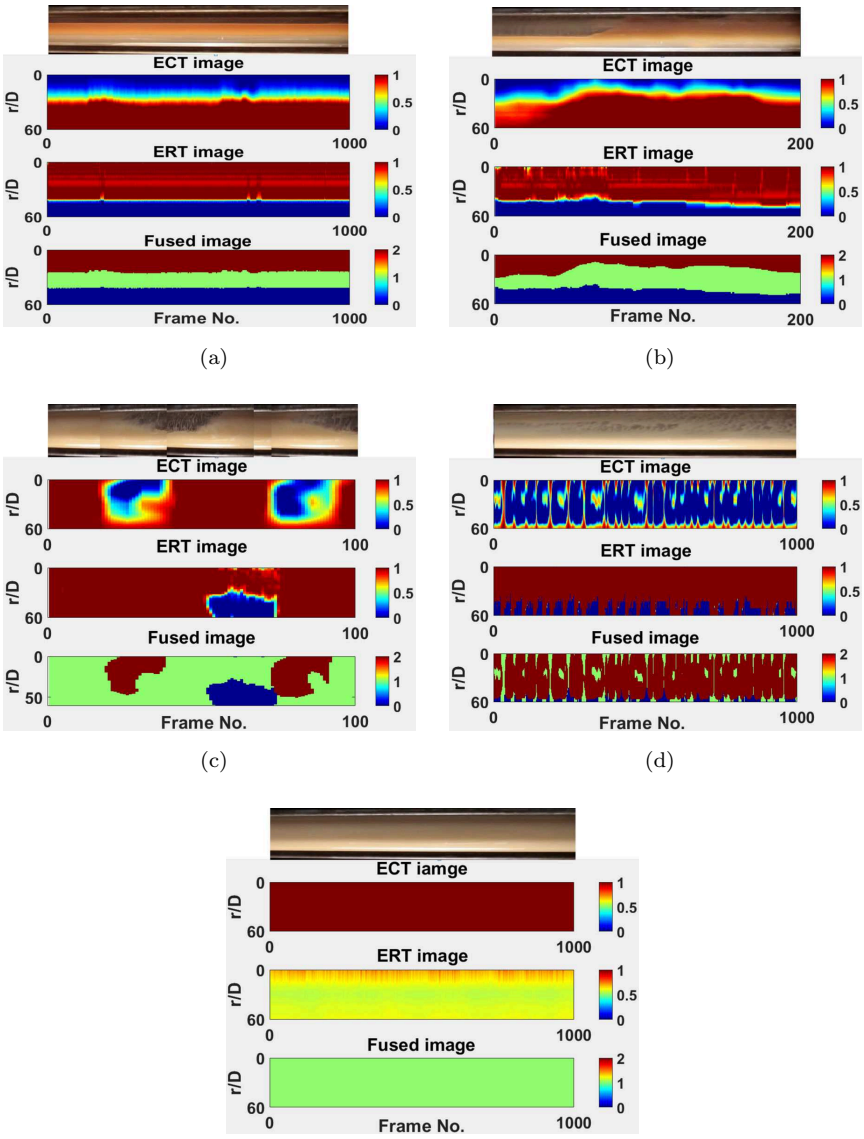

Figure 13: Visualisation results of WLR 50% for (a) stratified flow; (b) slug flow; (c) plug flow; (d) annular flow; and (e) bubbly flow.

imaging gas-oil-water flow at WLR 50%. There are small deviations from conditions as seen by the reference video logger as in Figure 13d, where the top liquid

Table 11: All examined flow conditions at WLR 50%.

Test No.	GVF %	ERT %	ECT %	Data fusion (%) gas	oil	water	Gammy %	Flow Regimes
1	40	74.37	41.20	40.75	27.59	31.66	47.74	stratified
2	60	74.37	40.42	39.90	28.47	31.63	62.58	stratified
3	85	87.03	48.04	42.51	38.08	19.41	85.70	stratified
4	95	93.83	74.34	84.23	8.75	7.02	94.21	stratified
5	98	97.94	91.88	98.47	1.53	0.00	97.79	transition
6	98.5	95.25	92.84	99.83	0.18	0.00	98.25	annular
7	25	74.05	36.37	36.23	31.20	32.57	33.39	slug
8	42	74.83	37.20	36.12	31.95	31.94	46.58	slug
9	60	87.66	46.43	40.73	36.54	22.73	64.53	slug
10	85	84.49	64.05	67.81	20.70	11.49	85.04	slug
11	95	84.34	75.99	84.36	10.61	5.03	95.02	transition
12	96.5	86.39	76.37	82.38	15.20	2.43	96.83	bubbly
13	10	74.53	29.56	28.54	38.21	33.25	19.98	transition
14	25	76.11	28.53	26.46	41.13	32.41	31.93	slug
15	40	74.68	23.72	19.83	57.91	22.27	47.47	slug
16	60	76.74	37.50	31.40	45.67	22.93	63.11	slug
17	85	79.27	43.75	31.57	41.91	26.53	86.28	transition
18	92	78.96	76.31	83.79	11.11	5.10	91.89	annular
19	15	58.55	11.95	9.78	82.53	7.70	23.16	plug
20	25	67.71	18.38	16.85	69.38	13.78	32.64	plug
21	35	72.63	72.68	26.81	57.70	15.49	42.28	plug
22	60	70.57	51.00	57.69	29.44	12.87	63.16	transition
23	75	70.25	70.81	81.36	13.12	5.52	77.33	annular
24	3	58.19	0.01	0.00	5.00	95.00	13.31	bubbly
25	5	59.27	0.01	0.00	100.00	0.00	14.97	bubbly
26	10	97.27	2.69	0.39	96.89	2.72	19.88	transition
27	15	95.26	7.68	2.57	92.73	4.70	24.23	transition
28	25	98.91	20.44	15.74	79.50	4.76	32.63	annular
29	35	69.78	35.96	42.60	50.97	6.42	41.83	annular

film is too thin to be detected by either modality. The system also struggles to image bubbly flow in Figure 13e, due to the incapability of both ERT and ECT systems to identify small bubbles. It is worth noting that bubble flow is notoriously difficult to measure for all levels of commercially developed multi-phase measurement systems. This limitation has been realised and further work is being conducted to address the inability to display very small features on a tomogram display.

Figure 14 explains the quantitative results in terms of water and gas concentrations by different approaches. The results from the ERT-ECT systems show

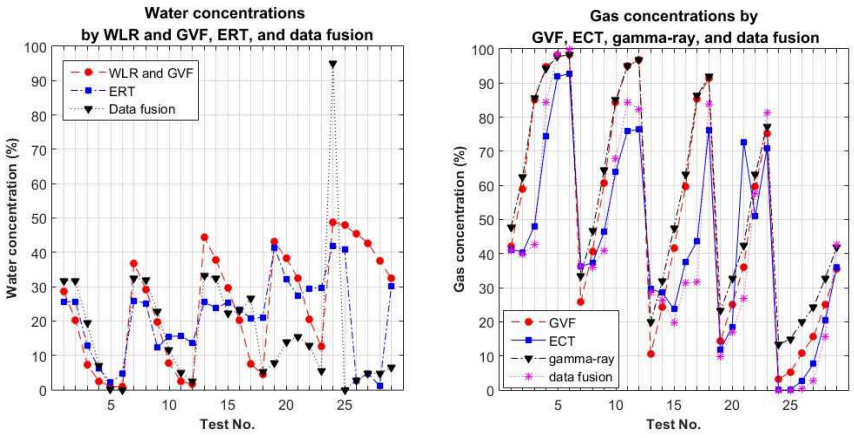

(a) (b)

Figure 14: Water (a) and gas (b) concentrations from different approaches at WLR 50%.

Table 12: Selected flow conditions for visualisation at WLR 75%.

	GVF (%)	Q_{water} (m^3/h)	Q_{oil} (m^3/h)	Q_{gas} (m^3/h)
Stratified flow	40	5.533	2.063	4.508
Slug flow	60	29.697	9.834	58.471
Plug flow	15	63.898	21.654	14.568
Annular flow	75	63.937	20.462	247.125
Bubbly flow	5	105.102	35.264	7.654

a good agreement with the ones using WLR and GVF. It is noticeable that the quantities are also in accordance with the visualisation. That is, the deviation of gas concentration from the references becomes significant for bubbly flow which, in turn, affects the accuracy of the water concentration.

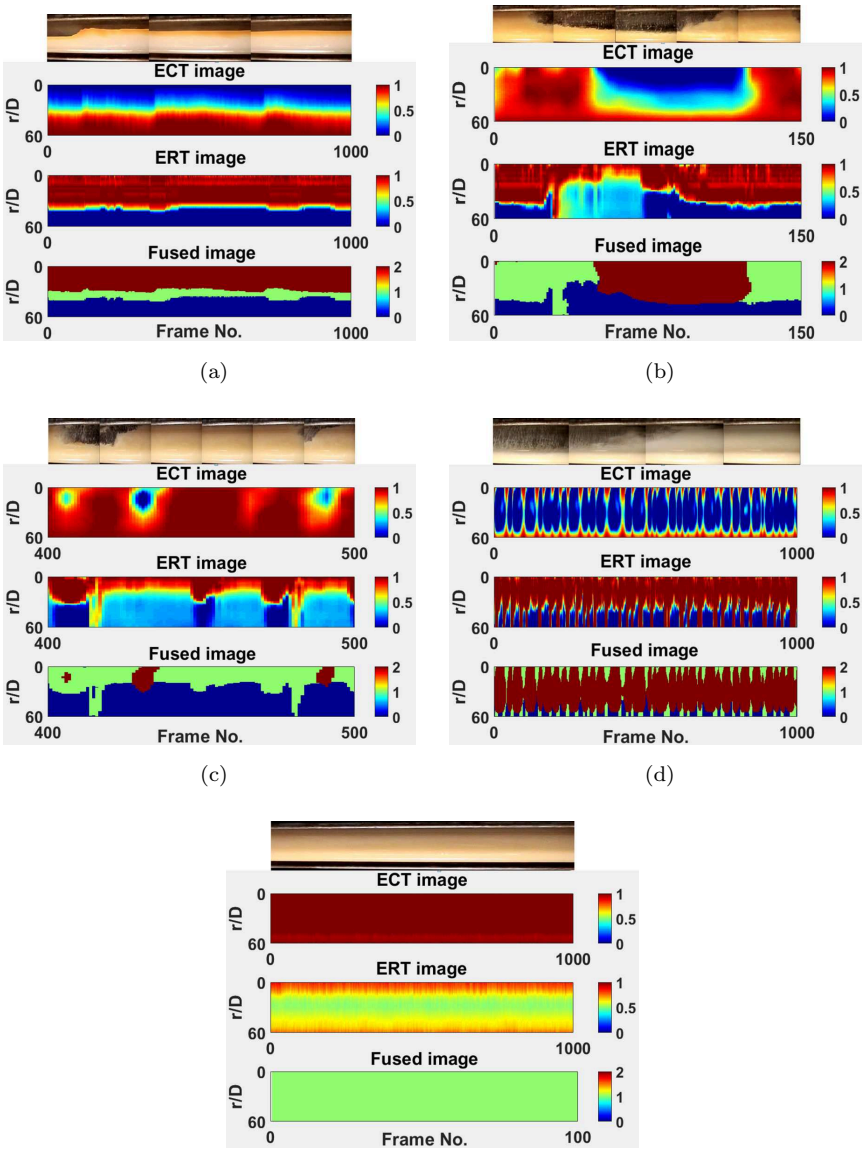

Figure 15: Visualisation results of WLR 75% for (a) stratified flow; (b) slug flow; (c) plug flow; (d) annular flow; and (e) bubbly flow.

Table 13: All examined flow conditions at WLR 75%.

Test No.	GVF %	ERT %	ECT %	Data fusion (%) gas	oil	water	Gammy %	Flow Regimes
1	40	71.25	48.21	48.43	15.93	35.64	40.34	stratified
2	60	73.26	49.31	49.68	16.61	33.71	61.77	stratified
3	85	87.34	64.65	63.42	14.84	21.74	87.68	slug
4	95	86.08	73.79	77.95	1.84	20.21	93.73	transition
5	98	85.76	80.18	88.13	0.10	11.78	97.31	transition
6	98.5	85.76	82.01	90.22	0.01	9.77	98.23	annular
7	25	63.31	38.41	39.24	20.16	40.60	29.17	slug
8	42	73.42	44.56	43.74	19.70	36.56	44.77	slug
9	60	84.18	55.71	53.20	20.34	26.45	66.04	slug
10	85	83.23	67.50	70.95	6.78	22.28	84.79	slug
11	95	84.49	79.32	86.82	1.61	11.58	94.58	transition
12	96.5	83.86	81.85	90.43	0.96	8.61	96.28	annular
13	10	53.55	18.84	9.64	46.24	44.12	14.86	slug
14	25	64.34	24.28	18.44	38.56	43.00	27.72	slug
15	40	74.68	31.59	27.01	29.54	43.45	43.50	slug
16	60	79.77	43.82	40.45	28.76	30.79	61.04	slug
17	85	82.91	74.42	82.19	5.31	12.49	86.08	annular
18	92	80.70	80.50	90.09	2.69	7.23	92.36	transition
19	5	54.24	1.62	0.06	36.47	63.47	10.33	plug
20	15	52.31	8.31	3.41	36.48	60.11	18.95	plug
21	25	70.47	17.27	14.60	32.92	52.49	28.37	transition
22	60	70.73	51.38	54.43	29.14	16.44	61.32	annular
23	75	70.57	68.52	78.96	12.11	8.93	75.31	annular
24	5	60.40	0.76	0.00	99.52	0.48	10.11	bubbly
25	15	74.00	3.95	0.67	94.61	4.71	19.54	plug
26	35	71.70	18.11	5.41	81.39	13.20	38.58	plug

3.5. WLR 75%

Similar to the results at WLR 50%, the ones at WLR 75 % reveal the certain capability of the dual-modality system to qualify and quantify gas-oil-water flow. The demonstration with regard to visualisation is in Figure 15, and the selected conditions are in Table 12 from Table 13. The results have comparable patterns with the ones at WLR 50%. That is, the visualisation of stratified flow (Figure 15a), slug flow (Figure 15b), plug flow (Figure 15c), and annular flow (Figure 15d) is in good agreement with the references, but not for bubbly flow (Figure 15e). As far as water and gas concentrations are concerned, the data fusion approach outperforms individual tomographic system, as illustrated in Figure 16.

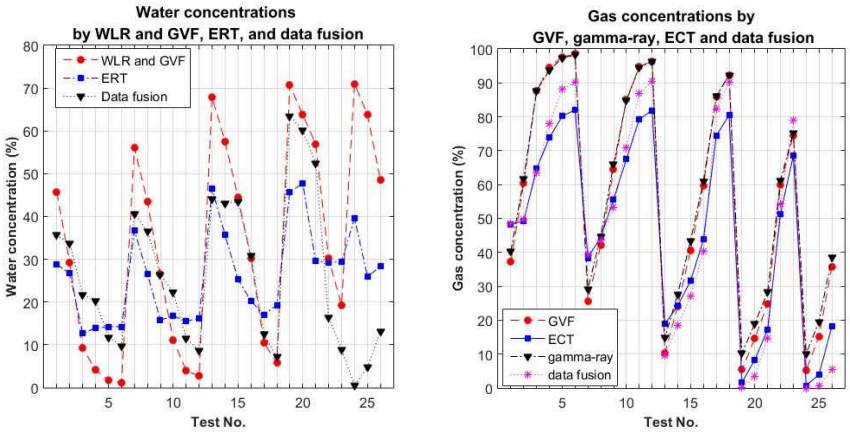

(a) (b)

Figure 16: Water (a) and gas (b) concentrations from different approaches at WLR 75%.

Table 14: Selected flow conditions for visualisation at WLR 90%.

	GVF (%)	Q_{water} (m^3/h)	Q_{oil} (m^3/h)	Q_{gas} (m^3/h)
Slug flow	35	76.601	8.438	45.577
Plug flow	15	76.329	8.485	16.158
Annular flow	92	36.563	4.130	455.277
Bubbly flow	3	126.374	13.932	4.716

In contrast to the reported performance of the ECT in [25], i.e. the ECT cannot image the flow with WLR beyond 40%, both images and figures prove that the ECT is still functioning at WLR 75%.

3.6. WLR 90%

Due to the unavailability of stratified flow, the visualisation for WLR 90% contains other four flow regimes from in total 21 flow conditons (Table 15), , with the conditions presented in Table 14. The flow is visualised by the

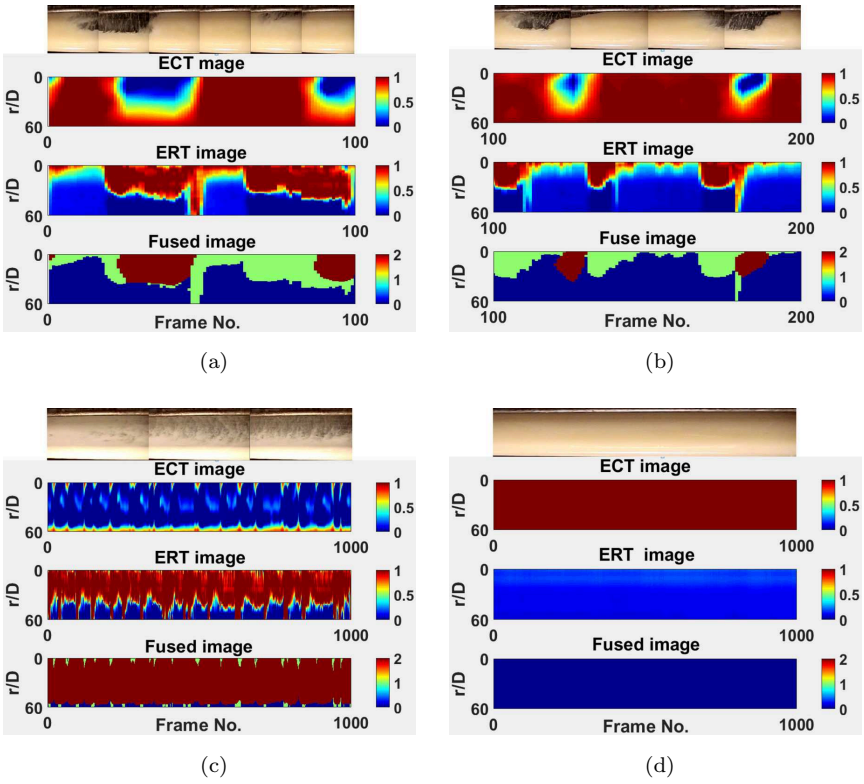

Figure 17: Visualisation results of WLR 90% for (a) slug flow; (b) plug flow; (c) annular flow; and (d) bubbly flow.

ECT, the ERT, and the data fusion approach, as depicted in Figure 17, and similar results occur with the given conditions. Figure 18 compares water and gas concentrations by different approaches. It is noted that the ECT is still operational at WLR 90%.

3.7. WLR 100%

When WLR is 100%, flow becomes a gas-water two-phase flow. It was observed that the ECT was still able to produce some tomograms, although they were distorted. Consequently, the images are only generated by the ERT, as demonstrated in Figure 19. For all engaged flow conditions shown in Table 16 selected from 23 different conditions in Table 17, the ERT tomograms are rea-

Table 15: All examined flow conditions at WLR 90%.

Test No.	GVF %	ERT %	ECT %	Data fusion (%) gas	oil	water	Gammy %	Flow Regimes
1	25	58.23	31.71	31.68	21.12	47.20	26.22	transition
2	42	66.30	39.28	37.87	19.78	42.35	42.39	transition
3	60	74.68	50.05	46.90	16.78	36.33	61.86	transition
4	85	71.52	65.35	65.09	22.06	12.85	84.56	slug
5	95	84.18	81.17	88.33	1.44	10.23	94.77	annular
6	96.5	84.18	83.68	91.59	0.85	7.55	7.16	annular
7	10	47.42	14.07	9.25	48.15	42.59	12.29	slug
8	25	62.35	19.93	17.38	28.82	53.81	26.82	slug
9	40	73.73	28.52	25.43	22.77	51.80	42.02	slug
10	60	78.55	41.75	40.23	22.98	36.79	58.88	slug
11	85	83.23	69.82	75.40	9.82	14.79	85.29	annular
12	92	78.96	79.43	89.02	3.33	7.65	91.61	annular
13	5	41.67	2.74	0.23	14.03	85.75	7.16	transition
14	15	52.74	9.71	4.86	19.46	75.68	17.62	plug
15	25	67.57	17.77	14.01	21.85	64.14	27.05	slug
16	35	68.99	20.15	16.89	25.76	57.35	35.86	slug
17	60	68.51	44.05	45.25	29.37	25.38	61.80	slug
18	75	68.31	65.61	76.23	15.52	8.25	76.28	annular
19	3	12.70	0.05	0.00	0.00	100.00	5.23	bubbly
20	15	64.05	0.45	0.00	26.55	73.45	16.70	bubbly
21	35	67.66	17.40	0.73	57.51	41.77	37.10	bubbly

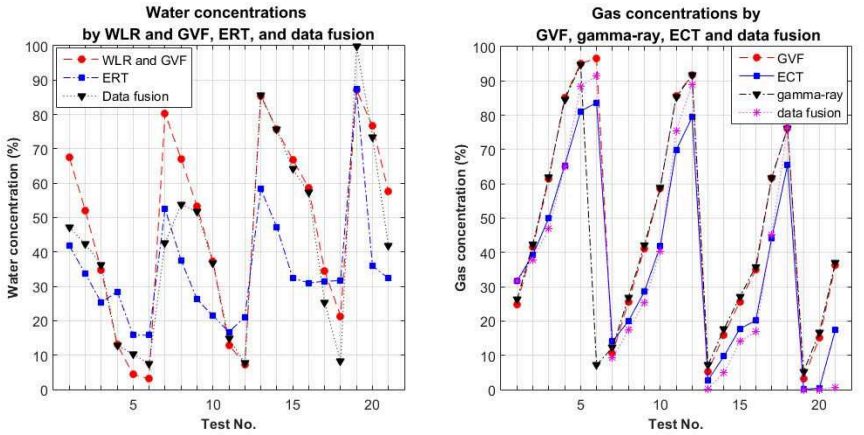

(a) (b)

Figure 18: Water (a) and gas (b) concentrations from different approaches at WLR 90%.

sonable, which is, as well, proven by the gas concentration in Figure 20.

Table 16: Selected flow conditions for visualisation at WLR 100%.

	GVF (%)	Q_{water} (m^3/h)	Q_{gas} (m^3/h)
Stratified flow	82	2.891	12.883
Slug flow	25	138.896	47.193
Plug flow	35	85.272	46.084
Annular flow	98.5	7.501	507.037
Bubbly flow	5	139.348	7.250

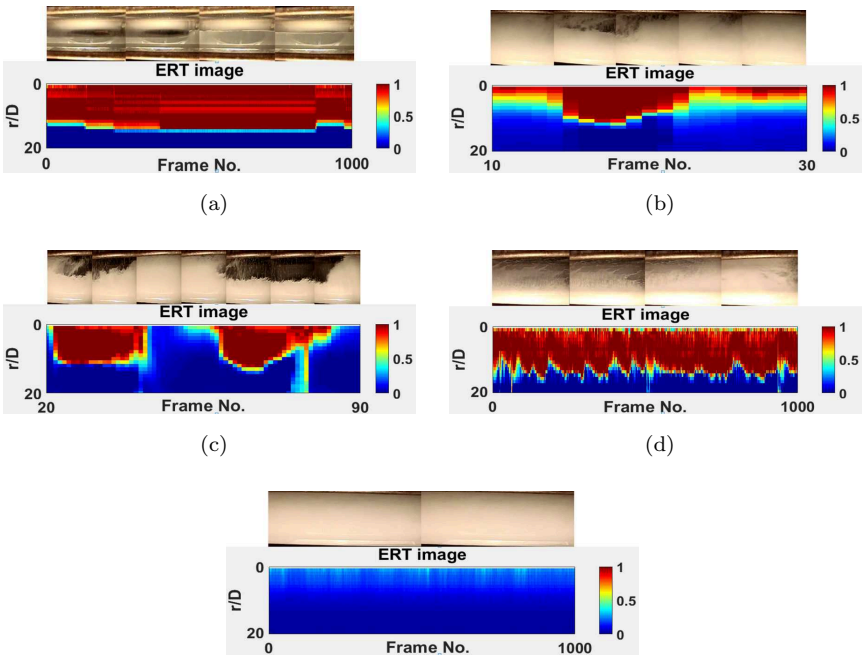

Figure 19: Visualisation results of WLR 100% for (a) stratified flow; (b) slug flow; (c) plug flow; (d) annular flow; and (e) bubbly flow.

Table 17: All examined flow conditions at WLR 100%.

Test No.	GVF %	ERT %	ECT %	Data fusion (%) gas	oil	water	Gammy %	Flow Regimes
1	82	75.29	x	x	x	x	80.78	stratified
2	97	84.81	x	x	x	x	96.01	stratified
3	99.4	81.33	x	x	x	x	99.20	annular
4	60	60.67	x	x	x	x	59.90	stratified
5	95	83.70	x	x	x	x	94.11	stratified
6	98.5	78.32	x	x	x	x	98.20	annular
7	42	55.77	x	x	x	x	41.97	slug
8	85	76.58	x	x	x	x	85.11	slug
9	95	81.79	x	x	x	x	94.64	annular
10	96.5	73.29	x	x	x	x	96.34	annular
11	25	52.85	x	x	x	x	24.73	slug
12	60	70.41	x	x	x	x	59.80	slug
13	92	68.31	x	x	x	x	91.90	annular
14	15	50.82	x	x	x	x	15.17	plug
15	35	57.16	x	x	x	x	34.66	plug
16	60	61.03	x	x	x	x	58.97	stratified
17	75	71.87	x	x	x	x	74.82	stratified
18	3	6.21	x	x	x	x	3.50	bubbly
19	5	8.50	x	x	x	x	4.91	bubbly
20	10	21.31	x	x	x	x	9.48	bubbly
21	15	35.94	x	x	x	x	14.23	slug
22	25	52.30	x	x	x	x	25.06	slug
23	35	56.57	x	x	x	x	33.87	slug

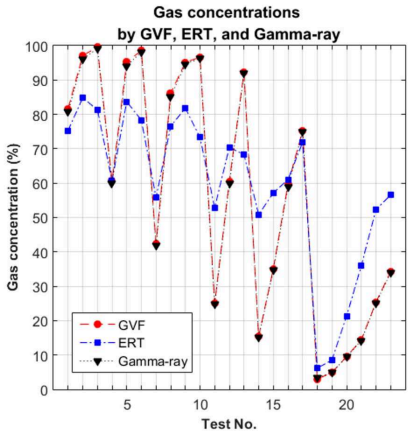

Figure 20: Gas concentrations from different approaches at WLR 100%.

4. Discussion

4.1. ECT system

The results in Section 3 demonstrate the capability of the applied ECT system to visualise multiphase flow in a horizontal pipeline. Compared to the reported suitability of the ECT system for the flow with WLR less than 40%, i.e. oil-continuous flow [25], the results clearly prove the capability of the ECT system can be extended to 90% WLR, with appropriate taking of reference.

When the flow structure is relatively simple, i.e. stratified flow and slug flow, and the flow is with relatively low or moderate flowrate, i.e. water and oil are not fully mixed, the ECT can detect the interface between gas and liquid, with great accuracy, such as the ones in Figure 7a and Figure 13b, etc. As for annular flow, the ECT is still able to image it with certain accuracy, e.g. in Figure 7d and Figure 11b. It is also able to detect the change in thickness of the top liquid film, as in Figure 11b. Nevertheless, it has to be pointed out that when the thickness is below the resolution of the ECT system, the film is undetectable, as in Figure 9c. Moreover, there are some ECT tomograms, e.g. Figure 15d, that depict a strange phenomenon, i.e. some liquid is at the centre of the pipe, which might be caused by the liquid droplets at the centre. As far as bubbly flow is concerned, when gas is fully dispersed in liquid, the ECT fails to extract tiny bubbles due to their size being below the ECT's resolution, whereas the quantitative results present that gas concentration can be extracted by the ECT.

With the reference method addressed in Section 3 and the ECT system provide by an industry, the system is able to manage three phase flows over the test conditions. However, as the consequence of the high complex permittivity of water and the use of the relative low permittivity of mixture of oil and water at specific WLR as reference, it may contribute to the error of the concentration from ECT. Nerveless, this did not present a significant impact on visualisation.

4.2. ERT system

For the examined WLR values, th deployed ERT system has a good agreement with the report [25]. That is, it is capable of handling gas-oil-water flow with WLR above 40%, i.e. water-continuous flow. Nonetheless, it was senn that the applied ERT system managed to image stratified and slug flow when WLR was at 25%, although the measured quantities had a large discrepancy to the reference values.

Within the effective WLR range, the ERT produces similar results compared with the ones using the ECT. When flow structure is simple and total flowrate is relatively low, the interface between conductive (water) and non-conductive (gas and oil) is clearly addressed. For stratified, slug, and plug flow, the boundaries are relatively sharp and reasonable, compared with related video log; whereas when water and oil are mixed together, the performance of the ERT deteriorates. The ERT was unable to image the top liquid film for engaged annular flow, due to the limitation of the ERT with respect to the spatial resolution. It is also noticed that there is an overestimate of the thickness of the bottom liquid film, which may result from the disturbance of the oil phase since the oil phase is supposed to be fully dispersed in the water phase for annular flow. Similar to the ECT, the ERT has no ability to identify dispersed tiny bubbles in bubbly flow, and hence no bubbles are seen in the ERT tomograms for bubbly flow. But it still presents water concentration even though tiny bubbles disappear in the images.

4.3. Dual-modality electrical tomographic systems

On the basis of the performance of the ERT and ECT, the dual-modality ERT-ECT systems are an effective method when characterising gas-oil-water horizontal flow of WLR between 40% and 90%, in accordance with the capabilities of the ERT and the ECT as single modality. Within this range, single-modality electrical tomography struggles to provide sufficient and accurate information to decompose the phases in the flow, whereas the integrated systems complement the limitations of either system by fusing the data from

both modalities. In contrast, when WLR is out of the range, the systems cannot provide complementary information by fusing the data from each modality.

By applying the threshold-based data fusion approach, individual phases are distinguished, and therefore visualised using different colours. In principle, the gas concentration by the fusion is determined by Ethe CT result, whereas the water concentration by the fusion depends on the ERT results. In consequence, the accuracy of the data fusion relies on the resolution of the ECT and the ERT. When total flowrate is relatively low, i.e. stratified flow and slug flow, both qualification and quantification are in great agreement with the references. In contrast, the performance of data fusion deteriorates when either modality cannot perform well, especially in terms of visualisation. A typical example is bubbly flow, in which both ERT and ECT are incapable of locating tiny bubbles, and hence the fused images provide little clues about tiny bubbles, although concentration information is still presented.

Overall, the application of the dual-modality electrical tomography results in more accurate quantities of phase concentrations within its functional range, compared to the ERT and ECT as a single modality. However, it is also noted that under some extreme conditions, e.g. bubbly flow, data fusion results are not as good as those by individual modality. As for gas concentration, the results by data fusion outperform those by the ECT alone, except on bubbly flow. This is essentially because of the limit of the ECT in this flow. On the other hand, the comparisons of water concentrations by different approaches indicate that the ERT results are not always as good as expected, especially at lower WLR, which reflects the negative effect of the oil phase as an additional non-conductive phase on the ERT. The quantities, however, become better after data fusion, despite there being extreme cases where the ERT outperforms data fusion, such as bubbly flow.

Despite the error caused by the above data fusion, it is worth noting that measurement uncertainty does play an important role. The measurement uncertainty mainly comes from two sources: one is systematic error, and the other is random noise. It is usually believed that about the 5% of systematic er-

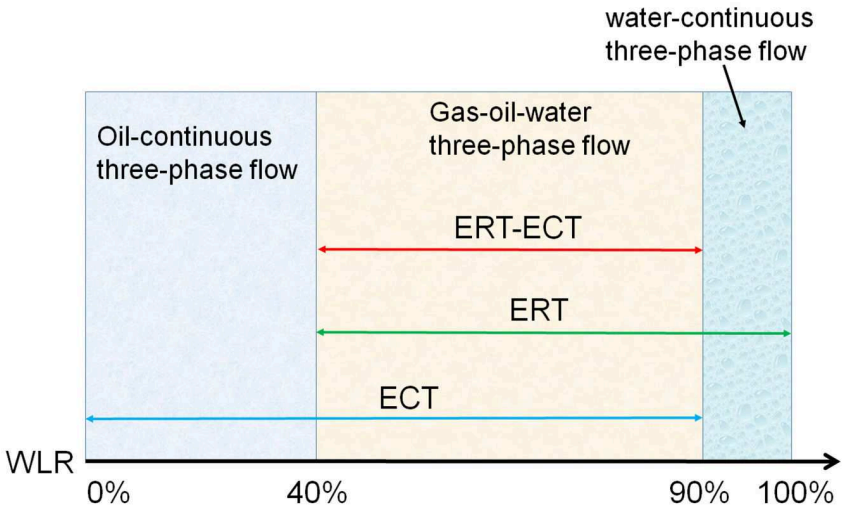

Figure 21: Capability of the ERT-ECT system against WLR.

ror comes from hardware [20], which could be introduced by the imprecision of sensing electronics and A/D conversion, improper compensation to temperature and/or ionic concentration changes etc. and also the artificial error from imaging reconstruction. Consequently, the ERT-ECT systems could introduce up to 10% systematic error but could be even higher as discussed in below section. Random noise, on the other hand, is generally as a consequence of uncontrollable and unrepeatable factors, such as flow instability, , electricity crosstalk, and so on. The uncertainty due to random noise could be 5% but can be reduced with the cost of increasing sampling number. Together the potential systematic error with the random noise, the final uncertainty of the mean concentration measurements could be up to 10-15%, which is linearly transferred by the image reconstruction algorithm employed in the study.

5. Conclusion

The experimental results demonstrate the overall capability of the dual-modality ERT-ECT systems in the domain of gas-oil-water flow characterisation. From the hardware perspective, the systems have proved to be effective, robust,

and reliable for the purpose of multiphase flow visualisation and measurement. Likewise, the images and numbers further substantiate the conclusion from the viewpoint of data processing. In WLR 0%-90%, the ECT is able to produce acceptable tomograms to reflect the distribution of gas phase and liquid phase, whereas the ERT is able to deal with the flow of WLR [40%, 100%] to distinguish gas and oil as conductive phase from water as a non-conductive phase. As a dual-modality system, the ERT-ECT can quantify and qualify the flow of WLR within [40%, 90%]. The capabilities of the ERT-ECT systems as single- and dual-modality are depicted in Figure 21.

Despite the advantages, there are still some aspects to be addressed in the future. First of all, further experiments should be carried out to make the evaluation more thorough. For example, WLR between 30% and 50% should be covered to determine the lower bound of the effective range for the systems. Moreover, a cross-correlation method should be applied to quantify the flowrate of each phase, so that the comparisons with GVF and WLR are more meaningful and accurate. The quantification of velocity would also contribute to study slip characteristics between each phase.

An essential impact on the performance of the ERT/ECT concentration measurement is the spatial resolution of the concentration tomograms. The systems utilised in this study have relatively low resolution due to the application of single-step linear back-projection (LBP) [17], which presented significant offsets at large GVFs. Advanced reconstruction algorithms, e.g. sensitivity theorem based conjugate gradients (SCG) [18] and the iterative Landweber method [19], could be applied to improve the resolution of the tomograms, which in turn improves the final results, especially as the data-processing speeds develop over time. The water component also impacts the performance of ECT. In addition, the change of continuous phase from oil to water clearly impacts on the performance of ERT/ECT, respectively. However, the concentration offsets at a low GVF may presents the nature difference from GVF due to the impact of slip velocity between gas and liquid phase presented at the test section.

The improvement of data fusion methodology is also worthy of more effort.

Although a threshold-based approach is effective, little effort has been made on a comprehensive evaluation of the impact of the selected threshold values on the final fused results. In addition, advanced fusion algorithms, e.g. fuzzy clustering [11], requires more computational power. Data fusion may mature into a process that can support the development, operation, and optimisation of multiphase flow measurement technology.

Last but not least is artificial errors during data fusion due to the registration process on spatial and temporal dimensions could be removed by the advanced design of hardware. For instance, the systems in [12, 14] are able to obtain both conductivity and permittivity information simultaneously, and thus the temporal registration in the fusion process is no longer necessary thereby reducing partial errors caused by the temporal interpolation during the registration.

Acknowledgment

The authors acknowledge the support by European Metrology Research Programme (EMRP) project Multiphase flow metrology in the Oil and Gas production jointly funded by the European Commission and participating countries within Euramet and the European Union.

References

[1] G. Hewitt, Three-phase gas-liquid-liquid flows in the steady and transient states, Nuclear Engineering and Design 235 (1012) (2005) 1303 – 1316, festschrift Edition Celebrating the 65th Birthday of Prof. Richard T. Lahey, Jr.20th Anniversary of Biosensors and Bioelectronicsrd International Symposium on Two Phase Modelling. doi:http://dx.doi.org/10.1016/j.nucengdes.2005.02.023.

[2] K. E. Kee, A study of flow patterns and surface wetting in gas-oil-water flow, Ph.D. thesis, Department of Mechanical and Systems Engineering Russ College of Engineering and Technology Ohio University (2014).

[3] R. Thorn, G. Johansen, B. Hjertaker, Three-phase flow measurement in the petroleum industry, Measurement Science and Technology 24 (1) (2012) 012003.

[4] T. York, H. McCann, K. B. Ozanyan, Agile sensing systems for tomography, IEEE Sensors Journal 11 (12) (2011) 3086–3105. doi:10.1109/JSEN.2011.2164905.

[5] M. Wang (Ed.), Industrial Tomography Systems and Applications, Woodhead Publishing, 2015.

[6] C. Qiu, B. Hoyle, F. Podd, Engineering and application of a dual-modality process tomography system, Flow Measurement and Instrumentation 18 (56) (2007) 247 – 254, process Tomography and Flow Visualization. doi:http://dx.doi.org/10.1016/j.flowmeasinst.2007.07.008.

[7] B. T. Hjertaker, S. A. Tjugum, E. A. Hammer, G. A. Johansen, Multimodality tomography for multiphase hydrocarbon flow measurements, IEEE Sensors Journal 5 (2) (2005) 153–160. doi:10.1109/JSEN.2005.843903.

[8] E. N. dos Santos, T. P. Vendruscolo, R. E. M. Morales, E. Schleicher, U. Hampel, M. J. D. Silva, Dual-modality wire-mesh sensor for the visualization of three-phase flows, Measurement Science and Technology 26 (10) (2015) 105302.

[9] M. Zhang, L. Ma, M. Soleimani, Dual modality ect-mit multi-phase flow imaging, Flow Measurement and Instrumentation 46, Part B (2015) 240 – 254, special issue on Tomography Measurement & Modeling of Multiphase Flows. doi:http://dx.doi.org/10.1016/j.flowmeasinst.2015.03.005.

[10] M. Wang, J. Jia, Y. Faraj, Q. Wang, C. Xie, G. Oddie, K. Primrose, C. Qiu, A new visualisation and measurement technology for water continuous multiphase flows, Flow Measurement and Instrumentation 46, Part B (2015)

204 – 212, special issue on Tomography Measurement & Modeling of Multiphase Flows. doi:http://dx.doi.org/10.1016/j.flowmeasinst.2015.06.022.

[11] S. Yue, T. Wu, J. Pan, H. Wang, Fuzzy clustering based et image fusion, Inf. Fusion 14 (4) (2013) 487–497. doi:10.1016/j.inffus.2012.09.004.

[12] Q. Marashdeh, W. Warsito, L. S. Fan, F. L. Teixeira, A multimodal tomography system based on ect sensors, IEEE Sensors Journal 7 (3) (2007) 426–433. doi:10.1109/JSEN.2006.890149.

[13] J. Sun, W. Yang, A dual-modality electrical tomography sensor for measurement of gasoilwater stratified flows, Measurement 66 (2015) 150 – 160. doi:http://dx.doi.org/10.1016/j.measurement.2015.01.032.

[14] H. Ji, W. Tan, Z. Gui, B. Wang, Z. Huang, H. Li, G. Wu, A new dual-modality ect/ert technique based on c4d principle, IEEE Transactions on Instrumentation and Measurement 65 (5) (2016) 1042–1050. doi:10.1109/TIM.2016.2526758.

[15] A. P. James, B. V. Dasarathy, Medical image fusion: A survey of the state of the art, Information Fusion 19 (2014) 4 – 19, special Issue on Information Fusion in Medical Image Computing and Systems. doi:http://dx.doi.org/10.1016/j.inffus.2013.12.002.

[16] S. Corneliussen, J.-P. Couput, E. Dahl, E. Dykesteen, K.-E. Frysa, E. Malde, H. Moestue, P. O. Moksnes, H. T. Lex Scheers, Handbook of multiphase flow metering (2005).
URL http://nfogm.no/wp-content/uploads/2014/02/MPFM_Handbook_Revision2_2005_ISBN-82-91341-89-3.pdf

[17] C. J. Kotre, Eit image reconstruction using sensitivity weighted filtered backprojection, Physiological Measurement 15 (2A) (1994) A125.

[18] M. Wang, Inverse solutions for electrical impedance tomography based on conjugate gradients methods, Measurement Science and Technology 13 (1) (2002) 101.

[19] W. Q. Yang, L. Peng, Image reconstruction algorithms for electrical capacitance tomography, Measurement Science and Technology 14 (1) (2003) R1.

[20] M. Wang, F. J. Dickin, R. Mann, Electrical resistance tomography sensing systems for industrial applications, Chemical Engineering Communications 175 (1) (1999) 49–70. arXiv:http://dx.doi.org/10.1080/00986449908912139, doi:10.1080/00986449908912139.

[21] J. C. Maxwell, A treatise on electricity and magnetism, Vol. 1, Clarendon press, 1881.

[22] D. Millington, Eng58 multiphase flow metrology in oil and gas production - work package 4 (flow visualisation), Tech. rep., TUV NEL (2016).

[23] J. Jia, M. Wang, H. I. Schlaberg, H. Li, A novel tomographic sensing system for high electrically conductive multiphase flow measurement, Flow Measurement and Instrumentation 21 (3) (2010) 184 – 190, special Issue: Validation and Data Fusion for Process Tomographic Flow Measurements. doi:http://dx.doi.org/10.1016/j.flowmeasinst.2009.12.002.

[24] Q. Wang, M. Wang, K. Wei, C. Qiu, Visualization of gas-oil-water flow in horizontal pipeline using dual-modality electrical tomographic systems, IEEE Sensors Journaldoi:10.1109/JSEN.2017.2714686.

[25] Y. Li, W. Yang, Measurement of multi-phase distribution using an integrated dual-modality sensor, in: Imaging Systems and Techniques, 2009. IST '09. IEEE International Workshop on, 2009, pp. 335–339. doi:10.1109/IST.2009.5071660.